Title
Protein Moonlighting Revealed by Non-catalytic Phenotypes of Yeast Enzymes

Journal
Genetics, 208(1)

ISSN
0016-6731

Authors
Espinosa-Cantú, Adriana
Ascencio, Diana
Herrera-Basurto, Selene
et al.

Publication Date
2018

DOI
10.1534/genetics.117.300377

Peer reviewed

Protein Moonlighting Revealed by Noncatalytic Phenotypes of Yeast Enzymes

Adriana Espinosa-Cantú,* Diana Ascencio,* Selene Herrera-Basurto,* Jiewei Xu,† Assen Roguev,† Nevan J. Krogan,† and Alexander DeLuna*,1

* Centro de Investigación y de Estudios Avanzados del Instituto Politécnico Nacional, Unidad de Genómica Avanzada (Langebio), 36821 Irapuato, Guanajuato, Mexico and †Department of Cellular and Molecular Pharmacology, University of California, San Francisco, California 94158

ORCID IDs: 0000-0001-9386-5051 (A.E.-C.); 0000-0003-4808-1244 (D.A.); 0000-0002-9236-2804 (A.D.)

ABSTRACT A single gene can partake in several biological processes, and therefore gene deletions can lead to different—sometimes unexpected—phenotypes. However, it is not always clear whether such pleiotropy reflects the loss of a unique molecular activity involved in different processes or the loss of a multifunctional protein. Here, using *Saccharomyces cerevisiae* metabolism as a model, we systematically test the null hypothesis that enzyme phenotypes depend on a single annotated molecular function, namely their catalysis. We screened a set of carefully selected genes by quantifying the contribution of catalysis to gene deletion phenotypes under different environmental conditions. While most phenotypes were explained by loss of catalysis, slow growth was readily rescued by a catalytically inactive protein in about one-third of the enzymes tested. Such noncatalytic phenotypes were frequent in the Alt1 and Bat2 transaminases and in the isoleucine/valine biosynthetic enzymes Ilv1 and Ilv2, suggesting novel "moonlighting" activities in these proteins. Furthermore, differential genetic interaction profiles of gene deletion and catalytic mutants indicated that *ILV1* is functionally associated with regulatory processes, specifically to chromatin modification. Our systematic study shows that gene loss phenotypes and their genetic interactions are frequently not driven by the loss of an annotated catalytic function, underscoring the moonlighting nature of cellular metabolism.

KEYWORDS protein moonlighting; systems genetics; pleiotropy; phenotype; metabolism; amino acid biosynthesis; *Saccharomyces cerevisiae*

THE phenotypic impact of a mutation is among the most useful genetic tools, providing insights into the functions of genes in biological systems. Functional genomics has produced vast amounts of phenotypic data in different model organisms from yeast to mammals (Pollard 2003; Shalem *et al.* 2015; Norman and Kumar 2016). Still, deciphering the relationship between genotypes and phenotypes is a central challenge in systems genetics (Baliga *et al.* 2017). Screens based on gene deletion or RNA interference (RNAi) perturbations have shown that many genes are associated with multiple, and sometimes unexpected, traits (Dudley *et al.* 2005; Ohya *et al.* 2005; Hillenmeyer *et al.* 2008; Zou *et al.* 2008; Carter 2013; Deutschbauer *et al.* 2014; Garay *et al.* 2014). A deep understanding of the molecular bases of such genetic pleiotropy contributes to our understanding of gene evolution, development, and disease (Promislow 2004; Wagner and Zhang 2011; Guillaume and Otto 2012; Hill and Zhang 2012; Smith 2016; Ittisoponpisan *et al.* 2017).

Genetic pleiotropy resulting from protein depletion may arise either from the loss of a single molecular function that impacts many cellular processes, or from the loss of more than one molecular function carried out by a single polypeptide (Hodgkin 1998; Stearns 2010; Paaby and Rockman 2013). Proteins were originally considered to be monofunctional, with a single, highly specific molecular function, as proposed in the key and lock model [discussed in Piatigorsky (2007) and Copley (2012)]. Nowadays, different mechanisms of protein multifunctionality have been described (Kirschner and Bisswanger 1976; Copley 2003; Khersonsky *et al.* 2006).

Moonlighting proteins are defined as polypeptides with two or more independent molecular activities, which are not the result of gene fusion events (Jeffery 1999; Piatigorsky 2007).

doi: https://doi.org/10.1534/genetics.117.300377
Manuscript received October 9, 2017; accepted for publication November 6, 2017; published Early Online November 10, 2017.
Supplemental material is available online at www.genetics.org/lookup/suppl/doi:10.1534/genetics.117.300377/-/DC1.
[1]Corresponding author: Centro de Investigación y de Estudios Avanzados del IPN, Unidad de Genómica Avanzada (Langebio), Km 9.6 Libramiento Norte Carretera Irapuato-Leon, 36821 Irapuato, Guanajuato, Mexico. E-mail: alexander.deluna@cinvestav.mx

Such proteins can provide a selective advantage to an organism and are hotbeds for the evolution of molecular function (Jensen 1976; Piatigorsky 2007; Espinosa-Cantú *et al.* 2015; Jeffery 2015). In moonlighting enzymes, proteins exert other molecular functions (*e.g.*, a structural scaffold or transcription factor) independently of their catalytic activity. Indeed, the moonlighting behavior of enzymes is usually confirmed in mutants that lack catalysis but retain any other molecular activity. Protein moonlighting gives rise to molecules that link metabolism with the regulation of gene expression (Shi and Shi 2004; Commichau and Stülke 2008; Boukouris *et al.* 2016), cellular cross talk (Entelis *et al.* 2006; Hill *et al.* 2013; Torres-Machorro *et al.* 2015), pathogenesis, and disease (Yoshida *et al.* 2001; Sriram *et al.* 2005; Henderson and Martin 2013; Zanzoni *et al.* 2015).

Over 300 examples of moonlighting proteins have been characterized in Archaea, Prokaryotes, and Eukaryotes, from model to nonmodel organisms (Hernández *et al.* 2014; Mani *et al.* 2015). In the budding yeast *Saccharomyces cerevisiae*, over 30 moonlighting enzymes have been characterized, many of which are enzymes of core metabolic pathways [reviewed in Gancedo and Flores (2008)]. Some moonlighting proteins have been identified by function-specific screens (Zelenaya-Troitskaya *et al.* 1995; Hall *et al.* 2004; Chen *et al.* 2005; Scherrer *et al.* 2010). More recent studies have aimed to identify moonlighting proteins by computational approaches (Chapple *et al.* 2015; Hernández *et al.* 2015; Pritykin *et al.* 2015; Khan and Kihara 2016). Still, systematic strategies to directly identify protein moonlighting are currently missing, and most known examples have been recognized by chance. Hence, the question remains of how frequent the moonlighting phenomenon is, and what are the underlying molecular mechanisms (Gancedo and Flores 2008; Huberts and van der Klei 2010; Khersonsky and Tawfik 2010; Hernández *et al.* 2014).

Here, we asked if annotated molecular activities are enough to explain the pleiotropic behavior of genes in yeast. We focused on enzymes involved in amino acid biosynthesis metabolism and quantified the contribution of catalysis to cellular phenotypes. To do so, we systematically compared the growth phenotypes of gene deletion (knockout) and site-directed loss-of-catalysis (catalytic) mutants in different growth conditions; high-quality data were obtained for 11 enzymes in our screen. While catalytic mutants recapitulated most gene deletion phenotypes, we found consistent phenotypes of several enzymes that did not depend on their annotated catalytic activity, suggesting moonlighting functions. We further explored the genetic interaction landscape of *ILV1* and showed that catalysis-independent genetic interactions fell into discrete functional groups. In doing so, we shed light on the cellular processes in which Ilv1 is involved independently of its threonine deaminase activity.

Materials and Methods

Strains, plasmids, and media

The parental *S. cerevisiae* strain used for gene replacement was Y8205 (*MAT*α *can1*Δ::STE2pr-Sp_his5 *lyp1*Δ::STE3pr-LEU2 *his3*Δ *leu2*Δ *ura3*Δ). Because strains from the yeast deletion collection may bear nonlinked mutations and aneuploidies (Hughes *et al.* 2000), all gene knockouts were generated *de novo* on an intact isogenic parental background. For gene replacement, the *nat*- or *hph*-resistance cassettes were amplified from pAG25 or pAG32, respectively. Phenotypic complementation of enzyme-coding genes included in the phenotypic screen ($GENE_i$) was done by transforming knockout strains (Y8205 $gene_i\Delta$::*nat*) with centromeric plasmids bearing (1) the intact $GENE_i$ sequence (resulting in strain WT_i), (2) the $gene_i$ catalytic mutant (CM_i strain), or (3) the empty plasmid (KO_i strain). Centromeric low copy number plasmids were from the MoBY-ORF collection of open reading frames from *S. cerevisiae* with their corresponding 5′-promoter and 3′-UTR sequences (Ho *et al.* 2009). The empty plasmid was p5586 MoBY with no yeast gene sequence. Strain Y8205 *his3*Δ::*nat* + p5586 was used as the "WT" (wild-type) reference (WT_{ref}). For all $GENE_i$s that have a $GENE_i$' paralog, plasmid transformations were also done on the Y8205 $gene_i\Delta$::*nat* $gene_i$'Δ::*hph* double-knockout background. Primer sequences for gene knockout and confirmation PCR were obtained from the Yeast Deletion Project (http://sequence-www.stanford.edu/group/yeast_deletion_project/deletions3.html). All strains used in this study are shown in Supplemental Material, Table S1.

Rich medium was Yeast-extract Peptone Dextrose (YPD); synthetic complete medium (SC) was 6.7 g/liter yeast nitrogen base without amino acids and 2% glucose (unless otherwise indicated), supplemented with 0.2% drop-out amino acid supplement mix from the Cold Spring Harbor Laboratory Manual (Amberg *et al.* 2005); see Table 1 for drop-out media used for auxotrophy tests. Antibiotic-resistant strains were grown in media supplemented with 100 μg/ml nourseothricin (ClonNAT; Werner BioAgents), 200 μg/ml G418 (Invitrogen, Carlsbad, CA), or 200 μg/ml hygromycin (Invitrogen); ammonium was replaced by 1 g/liter monosodium glutamic acid in SC medium with antibiotics.

Catalytic mutant design and site-directed mutagenesis

To generate yeast strains expressing enzymes with no catalytic activity, a single catalytic residue was targeted for each $GENE_i$ documented in the Catalytic Site Atlas (Furnham *et al.* 2014) or the MACiE Database (Holliday *et al.* 2012) (Table S2). Mutations were directed to an amino acid involved in the early stages of the reaction to prevent incomplete catalytic inactivation that could result in neomorphic phenotypes. If required, a second round of mutagenesis was directed to another residue involved in catalysis or in cofactor binding. Once a catalytic residue was selected, its conservation between the repository Protein Data Bank (PDB) and the query gene was established by sequence and structural alignments in PyMOL. In queries without PDB, models were obtained from the Swiss Model repository or generated automatically (Bienert *et al.* 2017). For each $GENE_i$, we substituted the catalytic residues to a residue with similar physicochemical characteristics, or to alanine.

Site-directed replacements of plasmid inserts were introduced by PCR with ~40 bp of overlapping primers with the mutation (Table S3). PCR was conducted in two stages: the

Table 1 Amino acid biosynthesis enzymes and catalytic mutants in this study

$GENE_i$	ORF	Molecular function[a]	Paralog	Auxotrophy	Mutation[b]
ALT1	YLR089C	L-Alanine:2-oxoglutarate aminotransferase	*ALT2* (65%)	Ala	K412A$^{(P)}$, **K412N**
ARG3	YJL088W	Ornithine carbamoyltransferase		Arg	C289A$^{(P)}$, C289M$^{(P)}$, H145A$^{(P)}$, H145N$^{(P)}$
ARG4	YHR018C	Argininosuccinate lyase		Arg	**H162A**, **H162N**
ARO3	YDR035W	DAHP synthase	*ARO4* (62%)	Trp, Tyr, Phe	**H281A**, **H281N**
ARO4	YBR249C	DAHP synthase	*ARO3* (62%)	Trp, Tyr, Phe	H282A$^{(P)}$, **H282N**
ARO7	YPR060C	Chorismate mutase		Phe	**E246A**, E246S$^{(P)}$
ASN1	YPR145W	Asparagine synthase (glutamine-hydrolyzing)	*ASN2* (95%)	Asp	**C2A**, **C2M**
ASN2	YGR124W	Asparagine synthase (glutamine-hydrolyzing)	*ASN1* (95%)	Asp	**C2A**, **C2M**
BAT2	YJR148W	Branched chain amino acid transaminase	*BAT1* (77%)	Leu, Val, Ile	**K202H**, **K202M**
HOM2	YDR158W	Aspartate-semialdehyde dehydrogenase		Thr, Met	C156A$^{(P)}$, C156M$^{(P)}$, S41A$^{(P)}$, S41G$^{(P)}$
HOM6	YJR139C	Homoserine dehydrogenase		Thr, Met	K223A$^{(NA)}$, **K223V**
ILV1	YER086W	L-threonine ammonia-lyase		Ile	**K109A**, K109N$^{(P)}$
ILV2	YMR108W	Acetolactate synthase *		Ile, Val	**E139A**, E139S$^{(P)}$
MET2	YNL277W	Homoserine *O*-acetyltransferase		Met	S168A$^{(P)}$, S168T$^{(P)}$, H430A$^{(P)}$, H430N$^{(P)}$
THR4	YCR053W	Threonine synthase		Thr	**K124A**, K124N$^{(P)}$
TKL1	YPR074C	Transketolase	*TKL2* (71%)	Trp, Tyr, Phe	**E418A**, **E418S**
TKL2	YBR117C	Transketolase	*TKL1* (71%)	Trp, Tyr, Phe	E418A$^{(P)}$, **E418S**
TRP1	YDR007W	PRA isomerase		Trp	**C17A**, **C17M**

[a] Molecular function annotation is from the *Saccharomyces* Genome Database. **ILV2* is also annotated with a flavin-adenine dinucleotide-binding activity. This was not considered a noncatalytic activity, given that it is a cofactor-binding function.

[b] Bold face indicates that the site-directed mutation resulted in an auxotrophic strain that was further used in this study; ^{P} indicates that the mutation resulted in a prototrophic strain; and ^{NA} indicates that the mutation was designed, but not obtained.

first stage included two independent reactions with the mutagenic forward or reverse primer in a final volume of 25 μl each (conditions below). PCR reactions were done with 5 ng/μl plasmid in a final mix of 25 μl with 1 unit of Phusion polymerase (Fermentas), 1× high-fidelity buffer, 0.2 μM dNTPs, and 0.5 μM primers. PCRs were first incubated for 3 min at 98°; then 15 cycles of 98° for 30 sec, 55° for 25 sec, and 7.5 min at 72°; with a final extension of 10 min at 72°. The second stage included 50 μl mixes of the two PCRs from the first stage, using the same parameters, followed by an overnight incubation at 37° with 0.5 μl of Dpn1 20,000 units/ml (Biolabs) to deplete original nonmutagenized plasmid sequences. A 5-μl sample of the digested PCR product was used to transform calcium-competent *Escherichia coli* BUN20 (Li and Elledge 2005). Selection was done in LB broth with 5 μg/ml tetracycline, 100 μg/ml kanamycin, and 12.5 μg/ml chloramphenicol. Plasmids from at least three clones from each transformation were sequenced with confirmation primers (Table S3). Confirmed mutated plasmids were used to transform yeast by lithium acetate (Schiestl and Gietz 1989), with selection for uracil prototrophy or geneticin resistance.

For amino acid auxotrophy confirmation by drop-spot assays, strains were grown for 36 hr in SC-uracil, cultures were diluted to OD_{600} = 0.5, and 3 μl of 10^0–10^6 dilutions were inoculated onto SC-aa and SC-uracil plates. Cultures were incubated at 30° during 72–96 hr and images were taken at two different time points for each set of strains.

Automated phenotypic characterization

Plasmid-transformed strains were inoculated into 100 μl of YPD with antibiotics in 96-well microtiter plates (Corning 3585) and grown without shaking at 30°. Saturated cultures (5 μl) were inoculated into 150 μl of different growth media for phenotypic analysis under different conditions (see below). Growth was monitored in an automated robotic system (Tecan Freedom EVO200) that integrates a plate carrousel (Liconic STX110), a plate reader (Tecan Infinite M1000), an orbital plate shaker, and a robotic manipulator arm (Garay *et al.* 2014). The equipment was maintained in an environmental room at constant temperature (30°) and relative humidity (70%). Absorbance at 600 nm (OD_{600}) was measured every 60–90 min after vigorous shaking and growth kinetics were followed for 24–30 hr. Unless otherwise noted, all experiments were performed in five independent biological replicates resulting from individual colonies from plasmid transformation.

Phenotypic characterizations were done under different growth conditions (C_j): YPD, SC, or the following environmental perturbations on YPD medium: pH 3, pH 8, 0.01% Sodium dodecyl sulfate, 5 mM Caffeine, 6% Ethanol, 100 mM $CaCl_2$, 20 μg/ml Benomyl, 1.4 mM H_2O_2, 1.6 μg/ml Amphothericin B, 0.04% Methyl methanesulfonate, 80 mM Hydroxyurea, 150 μg/ml Fluconazole, 0.4 M KCl, 1 M Sorbitol, 1 M Glycerol, 50 μM Menadione, and 150 μM Paraquat dichloride. Reagents were purchased from Sigma ([Sigma Aldrich], St. Louis, MO). These environments affect different cellular processes in yeast (Hampsey 1997; Dudley *et al.* 2005).

Data analysis

Growth kinetics were analyzed as in Warringer and Blomberg (2003) using Matlab. In brief, mean blank OD_{600} was subtracted to all OD_{600} values within the same plate; negative values were set to 10^{-4}. Nonlinearity at high OD_{600} values was corrected with the formula $OD_{corr} = OD_{600} + 0.449(OD_{600})^2 + 0.191(OD_{600})^3$. Smooth growth curves were obtained by eliminating all negative differential data points; smoothed OD_{corr} values were log10-transformed. A slope was calculated for each three consecutive time points in the growth curve. In a similar strategy to that of

Warringer and Blomberg (2003), doubling times (D) were calculated from the mean of the second and third maximum slopes of $log_{10}(ODcorr)$ as a function of time. Growth rate was defined as $r = ln(2)/D$. Mean growth rates ($\bar{r}$) and their SE from the independent replicates were calculated for each strain under each C_j condition. Relative growth rates (G) of KO_i and CM_i were defined as $\bar{r}(KO_i, C_j)/\bar{r}(WT_i, C_j)$ and $\bar{r}(CM_i, C_j)/\bar{r}(WT_i, C_j)$, respectively.

For classification of catalytic and noncatalytic phenotypes, the growth rates of knockout (KO_i) and catalytic mutants (CM_i) of each $GENE_i$ under each C_j condition were tested for the null hypothesis $\bar{r}(KO_i, C_j) \geq \bar{r}(CM_i, C_j)$ by a one-tailed Wilcoxon test (Matlab rank-sum), with the alternative hypothesis $\bar{r}(KO_i, C_j) < \bar{r}(CM_i, C_j)$.

A false discovery rate (FDR) approach (Benjamini and Hochberg 1995) was used to correct P-values for multiple testing; noncatalytic phenotypes were defined using a 5% FDR threshold and values above this cutoff were classified as catalytic. To avoid classification of marginal phenotypic effects, all cases where $\bar{r}(KO_i, C_j)/\bar{r}(WT_i, C_j) > 0.95$ were labeled as "no phenotype."

The catalytic contribution (CC) to the phenotypes of each $GENE_i$ under each condition j was defined as $CC_{i,j} = 1 - G_{CMi,j}/1 - G_{KOi,j}$, namely the ratio of the growth rates of catalytic mutant and knockout strains relative to the WT_i; $CC_{i,j} < 0$ (0.14% cases) and $CC_{i,j} > 1$ (0.042% cases) were bound to 0 and 1, respectively.

Differential epistasis profile analysis with genome-integrated mutants

We constructed the genomic-integrated variants of WT_{ILV1}, KO_{ILV1}, and CM_{ILV1}. The *nat* cassette was amplified using A1 and A2 primers (Table S4) with sequences 160 bp downstream of *ILV1*, and used to transform the parental Y8205 strain. DNA from the resulting strain (reference strain *ILV1-nat*) was used as a template for a PCR with primers ilv1-K109A and A2. The amplification product was transformed into Y8205 to obtain the catalytic mutant strain, *ilv1*^{K109A}*-nat*. The knockout strain, *ilv1*Δ::*nat*, was generated by replacing *ILV1* from the start codon to the same 160 bp downstream site using primers ILV1-MXF1 and A2.

Additionally, two control strains were constructed: an alternative knockout strain, *ilv1*Δ(bis)::*nat*, obtained by replacement of *ILV1*'s ORF from the first to the last codon (with oligos ILV1-MXF1 and ILV1-MXF2), and another reference strain, *NTR-nat*, with a resistance marker integrated at a neutral locus, obtained by insertion of the *nat* cassette 200 bp downstream of *ARO7* (oligos NTR-Nat-F and NTR-Nat-R).

Strains with mutations integrated to the genome were used for the differential epistasis profile analysis (Bandyopadhyay *et al.* 2010; Braberg *et al.* 2013). Reference, knockout, and catalytic mutant strains were mated to a collection of nonessential *MAT***a** *xxx*Δ::*kan* deletion strains. Seven technical replicates for each reference strain, *ILV1-nat* and *NTR-nat*, were included, and one replicate of each of the *ilv1*^{K109A}*-nat*, *ilv1*Δ::*nat*, and *ilv1*Δ(bis)::*nat* strains. After sporulation, each strain collection was triplicated, obtaining 21 replicates of each reference strain, and three technical replicates for each of the three mutant constructs. Haploid *MAT***a** strains bearing the two resistance markers (*nat* and *kan*) were selected and pictures were taken after 48 hr of incubation at 30° in double-marker selection medium, as described in Collins *et al.* (2010).

Genetic interaction scores (S-scores) were calculated from the sizes of the double-marker colonies as described, with the EMAP toolbox (Collins *et al.* 2010). S-scores account for the magnitude and the confidence of the genetic interaction. In brief, colony sizes were normalized by position and by the distribution of colony sizes in the plate. Given that genetic interactions are rare, the median of the normalized colony sizes of each plate and each array gene is used to calculate the expected double-marker colony size; the high number of technical replicates in reference strains *ILV1-nat* and *NTR-nat* were used to obtain robust data for such a calculation (Schuldiner *et al.* 2005; Collins *et al.* 2010). Data from normalized colony sizes above or below an establish threshold were eliminated (size > 1500; size < 5). Also, data from double-marker strains was filtered out if (1) the replicates presented high SE, (2) if the mean S-score of either reference strain were > 2 or < -3, or (3) if the array gene was close to the *ILV1* locus (50 kb), avoiding apparent negative S-scores due to genetic linkage. The SD of S-scores increases in a nonlinear manner with respect to its magnitude (Bandyopadhyay *et al.* 2010); therefore, to compare the S-scores from different epistasis profiles, we calculated the variance (σ) as a nonparametric function using a sliding window of S-scores with the polynomial $\sigma = 0.012x^2 - 0.095x + 0.502$, where x is de difference of the S-scores evaluated, with limits of σ at 2 (Bandyopadhyay *et al.* 2010).

Functional clustering and gene ontology (GO) term enrichment

Functional modules were obtained for genes—from noncatalytic and catalytic genetic interactions separately—according to their shared functional terms (GO terms and mutant–phenotype annotations, 1748 terms in total). To do so, the overall agreement between gene pairs was evaluated by Cohen's κ ($kappa = Pra(a) - Pr(e)/1 - Pr(e)$), where $Pra(a)$ is the relative observed agreement or the number of terms that a gene pair shares divided by the total number of terms in the matrix, and $Pr(e)$ is the probability of agreement by chance, calculated as the sum of probabilities for each member of the gene pair to be associated or not to each term. Gene pairs that showed $kappa > 0.35$ were used as cluster seeds; groups sharing $> 50\%$ of their genes were merged. The resulting gene modules were named based on the most common functional feature of genes in the module. Network representation was created using Cytoscape. GO term annotations and mutant–phenotype annotations were downloaded from the Yeast Genome Database (December 2016).

GO enrichment analyses were performed using GOrilla (Eden *et al.* 2009), with a target list compared to the specific

background list of genes tested. If specified, redundancy of GO terms was removed using REVIGO (Supek *et al.* 2011).

Data availability

All strains are available upon request. Table S1 contains a detailed description of all strains generated and used in this study. Table S3 and Table S4 describe all primers and their sequences. Phenotypic and genetic interaction data are provided in File S1 and File S2, respectively.

Results

Selection of enzyme-coding genes and catalytic mutant design

We set out to test in a systematic manner whether gene deletion phenotypes of enzymes from *S. cerevisiae* are caused by the loss of their catalytic activities. To this end, we designed an experimental strategy based on the comparison of the growth phenotypes of catalytic mutant strains (loss-of-function substitution of a single catalytic residue in an otherwise intact protein) and gene deletion strains (knockout, *i.e.*, no protein at all) (Figure 1). We concentrated our experimental analysis on genes related to metabolism—a powerful model cellular system for studying gene function (Segre *et al.* 2005; DeLuna *et al.* 2008; Szappanos *et al.* 2011)—and focused our screen on enzymes of amino acid biosynthesis, since loss of their catalytic function can be readily confirmed by amino acid auxotrophy. From the *Saccharomyces* Genome Database (http://www.yeastgenome.org), we selected 86 single-gene knockouts (or double knockouts for paralogous isoenzymes) resulting in an amino acid auxotrophy; histidine auxotrophy was not considered because the parental strain used has a *his3*Δ genotype. Our experiments were based on haploid knockout strains complemented with centromeric plasmids; hence, out of the 86 auxotrophic and viable strains, we further considered 56 genes that were part of the MoBY-ORF plasmid collection with coding sequences from *S. cerevisiae* with their corresponding 5′-promoter and 3′-UTR sequences (Ho *et al.* 2009). Next, we selected enzymes annotated with a single molecular function (Ashburner *et al.* 2000) (the catalytic activity) and with well-characterized enzymatic reaction mechanisms in the Catalytic Site Atlas (Furnham *et al.* 2014) or the MACiE Database (Holliday *et al.* 2012). This resulted in 18 genes, herein referred to as the $GENE_i$ set: *ALT1*, *ARG3*, *ARG4*, *ARO3*, *ARO4*, *ARO7*, *TKL1*, *TKL2*, *TRP1*, *ASN1*, *ASN2*, *ILV1*, *ILV2*, *BAT2*, *HOM2*, *HOM6*, *MET2*, and *THR4* (Table 1). Such enzymes perform a wide variety of reactions, represent diverse protein folds, and are involved in different amino acid biosynthetic pathways (Table S2).

To generate strains expressing $GENE_i$ proteins with no catalytic activity (catalytic mutant strain, CM_i), we replaced a single "essential" catalytic residue that directly participates in the catalysis (see *Materials and Methods*). We tested the loss of catalytic activity by auxotrophy of $gene_i\Delta$ strains bearing plasmids with site-directed mutations. Three out of the 18 $GENE_i$ enzymes (Arg3, Hom2, and Met2) were discarded

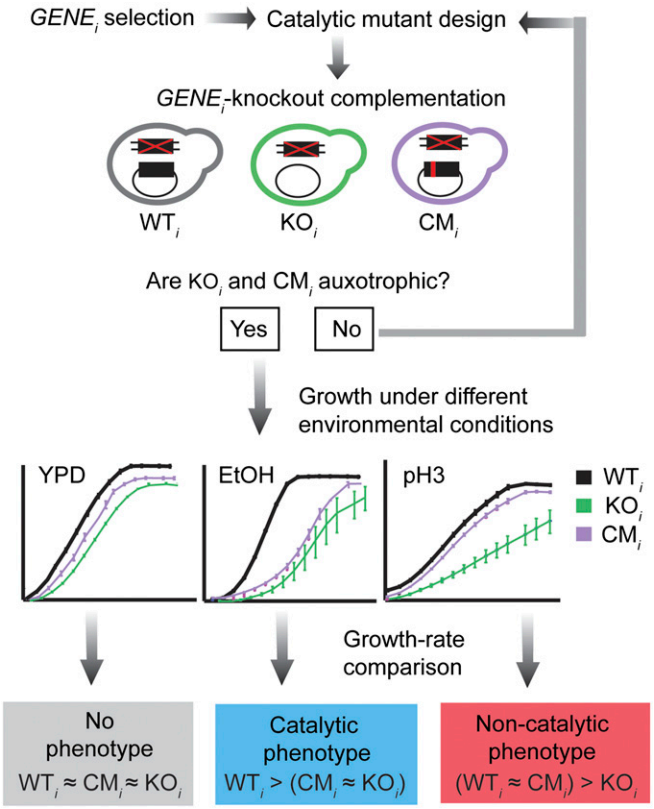

Figure 1 A systematic experimental strategy to dissect the molecular bases of enzyme-loss phenotypes. Enzyme-encoding genes ($GENE_i$) from amino acid biosynthesis metabolism were selected; residues involved in early catalysis were targeted for site-directed mutagenesis. Plasmid-borne wild-type (WT_i), gene knockout (KO_i), or catalytic mutant (CM_i) constructs were used to complement the corresponding $gene_i\Delta$ (deletion of $GENE_i$). Loss of catalytic function was confirmed by amino acid auxotrophy; growth of complemented strains was characterized under different environmental conditions. Growth rates were used to classify each case as no phenotype (gray), catalytic phenotype (cyan), or noncatalytic phenotype (red).

because no site-directed mutant tested resulted in loss of catalysis. All other catalytic mutants were unable to grow after long incubation in minimal medium (Figure 2A and Figure S1). Although substitution of residues that are considered essential for enzymatic function may not completely abolish catalysis but rather alter the catalytic mechanism (Peracchi 2001), the fact that catalytic mutant strains did not grow in the absence of amino acids indicates loss of the catalytic activity that is required for growth. Residual growth after 72 hr of inoculation was only observed in the *ilv2*^{E129A} catalytic mutant. Moreover, many of the loss-of-function point mutations used here had been thoroughly characterized elsewhere (Fisher and Eisenstein 1993; Schnappauf *et al.* 1997; DeBaBarre *et al.* 2000; Kingsbury *et al.* 2015).

Site-directed substitutions of protein amino acids may impact organismal fitness by different mechanisms, in addition to the loss of a specific function (Tokuriki and Tawfik 2009; Jeffery 2011; Song *et al.* 2014). Therefore, we inspected if particular amino acid replacements in the catalytic mutants accounted for dominant effects on fitness. To this end, we

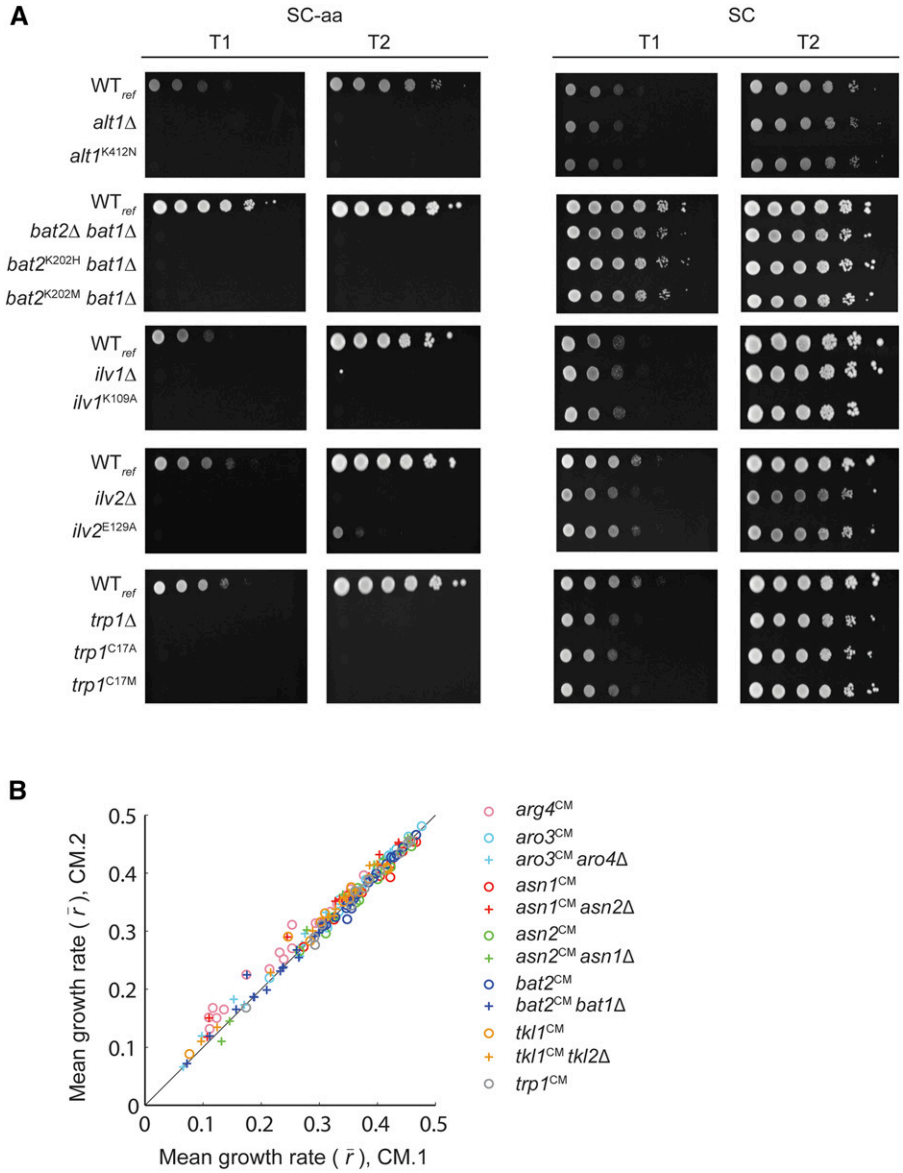

Figure 2 Complete loss of catalytic function with no additional dominant effects caused by specific residue replacements. (A) Drop-spot assays of auxotrophy. Culture dilutions were inoculated onto SC-aa (right) and SC-uracil (left) plates and incubated at 30°. Images correspond to growth after 48 hr (T1) and 96 hr (T2) for slow growers (*ALT1* and *BAT2*), or 24 hr (T1) and 72 hr (T2) for *ILV1*, *ILV2*, and *TRP2*. (B) Comparison of the mean growth rates under different environmental conditions (C_j) of catalytic mutant strains of $GENE_i$ for which two different catalytic mutants were generated, validated, and screened ($CM.1_i$ and $CM.2_i$; n = 165). WT, wild-type.

compared the growth phenotypes of different amino acid substitutions of the same catalytic residue for enzymes in which two confirmed catalytic mutant strains were available. Importantly, we observed high correlation of growth phenotypes between the two catalytic mutants characterized under different conditions ($r^2 = 0.98$; Figure 2B). Such high correlation was not observed after randomizing mutant pairs (Figure S2). Taken together, these results suggest that the phenotypes of catalytic mutants are not the result of residual activity, altered catalytic properties, or dominant effects of particular amino acid replacements, but are more likely due to complete loss of enzyme catalysis.

Quantitative analysis of the contribution of catalysis to phenotypes

For 15 $GENE_i$ enzymes with a confirmed loss-of-function, auxotrophic CM_i, we performed a large-scale phenotypic screen aimed to analyze the contribution of catalysis to the growth phenotypes of the corresponding gene knockout, KO_i. To this end, we monitored the growth kinetics of all strains (Table S1) in five biological replicates (independent plasmid-transformation clones), challenged to 19 different growth conditions, C_j (see *Materials and Methods*). For each experiment, we calculated the growth rate and filtered out atypically high rates with respect to the WT reference (WT_{ref}) grown in YPD ($< 0.4\%$ samples; Figure S3A). As expected, growth under environmental perturbations was slower than on YPD (Figure S3B). To avoid hypomorphic effects associated with the expression of a gene from a centromeric construct, which would complicate downstream analysis, we filtered out genes in which the gene-specific WT_i strains grew slower than the WT_{ref} (4 out of 15 genes; Figure S3C). In the final data set of 11 $GENE_i$ enzymes, growth of WT_i strains showed high correlation to the universal WT_{ref} strain ($r^2 = 0.905$; Figure S3D). As expected, the median growth rate of KO_i and CM_i strains was significantly lower than that of growth of the WT_i ($P < 10^{-15}$ and $P < 10^{-15}$,

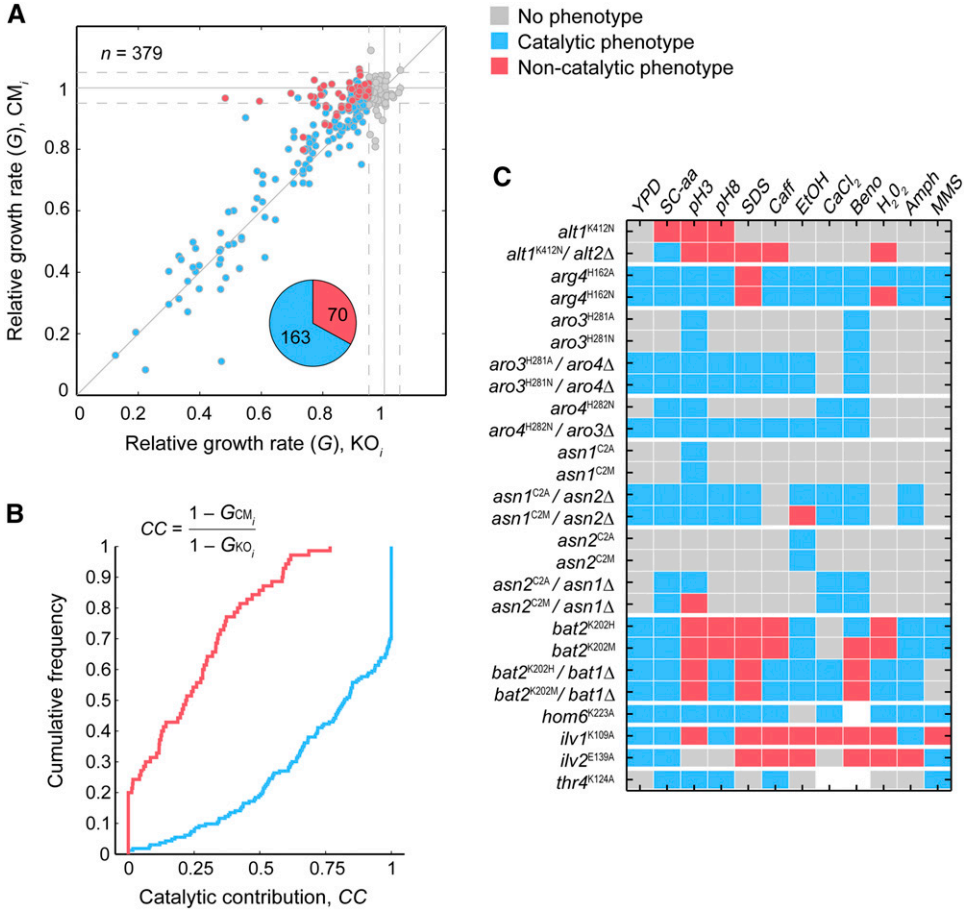

Figure 3 Noncatalytic phenotypes in biosynthetic enzymes from yeast. (A) Scatter plot of growth rates relative to WT_i (G) of gene knockouts KO_i (x-axis) and catalytic mutants CM_i (y-axis) of 11 $GENE_i$s characterized under different growth conditions. Growth phenotypes were defined as $G < 0.95$ (gray dots indicate no phenotype); based on growth rate differences (5% FDR), phenotypes were classified as catalytic (cyan) and noncatalytic (red). Pie chart shows the fraction of catalytic and noncatalytic phenotypes. (B) Cumulative distribution of the CC of the catalytic (cyan) and noncatalytic (red) phenotypes. (C) Figure shows the three phenotype categories of different $GENE_i$ (vertical axis; labels are names of CM_i strains) under different environmental perturbations C_j (horizontal axis). White indicates missing data points. Only 12 conditions for which data were obtained for most of the $GENE_i$ are shown (see Figure S5 for all conditions). Amph, 1.6 μg/ml Amphothericin B; Beno, 20 μg/ml Benomyl; Caff, 5 mM Caffeine; CC, catalytic contribution; FDR, false discovery rate; WT, wild-type.

respectively; one-tailed Wilcoxon rank-sum test). The complete phenotypic data set for the 11 $GENE_i$ enzymes under 19 environmental conditions is provided in File S1.

We classified the phenotypic data set in three groups based on the relative growth rates (G) of the KO_i and CM_i mutant strains: (1) no phenotype, (2) catalytic phenotype, and (3) noncatalytic phenotype. We found that in 38.6% out of 379 growth rate comparisons, the knockout had little or no effect ($G > 0.95$) (Figure 3A; no phenotype). We further classified the remaining 233 slow-growth phenotypes; for 70%, we found no significant difference between the growth phenotypes of catalytic and knockout mutants (catalytic phenotypes). Interestingly, in 30% cases, the catalytic mutant grew significantly faster than the corresponding knockout (5% FDR, one-tailed Wilcoxon rank-sum test). In such cases of noncatalytic phenotypes, at least part of the phenotype did not depend on the loss of enzymatic activity. We note that the fraction of noncatalytic phenotypes is sensitive to the choice of conditions, given that the growth phenotypes across conditions are not independent from one another (Dudley *et al.* 2005). We also note that catalytic mutant strains rarely grew better than the wild type (1% $G_{CMi} > 1.05$) or worse than the corresponding knockout strain (6.8% $G_{CMi} - G_{KOi} < -0.05$), which suggests that no structural defects or neomorphic phenotypes result from the site-directed mutations. Taken together, these results suggest that the loss of an additional molecular activity in the gene knockout—a moonlighting function—could contribute to the observed phenotype.

As noted above, we defined noncatalytic phenotypes as significant slow growth of the KO_i compared to the CM_i strain. Therefore, in noncatalytic phenotypes, at least part of the knockout phenotype is not explained by the loss of catalysis. To quantify the contribution of the loss of catalysis to the noncatalytic phenotypes, we established a CC factor, a result of the fraction of the magnitude of the knockout phenotype that was different to that of the catalytic mutant (see *Materials and Methods*). In this way, a CC value close to one means that catalysis solely explains the phenotype, while a value close to zero means that catalysis does not contribute to the gene knockout phenotype. We observed that, in the vast majority of the scored noncatalytic phenotypes, the loss of the catalysis explained less than half of the knockout phenotype ($CC = 0.5$), and in 20% of the cases catalysis did not contribute at all to the gene deletion phenotype ($CC = 0$; Figure 3B). As expected, the median CC in scored catalytic phenotypes was high ($CC = 0.82$; Figure 3B). These results underscore that, for an important number of observed phenotypes, the effect is largely driven by the loss of a molecular function other than the known catalysis of the enzyme.

Most noncatalytic phenotypes were concentrated in deletions of *ALT1*, *BAT2*, *ILV1*, and *ILV2* (Figure 3C; see Figure S4 for KO_i and CM_i phenotypes and Figure S5 for the entire set of conditions

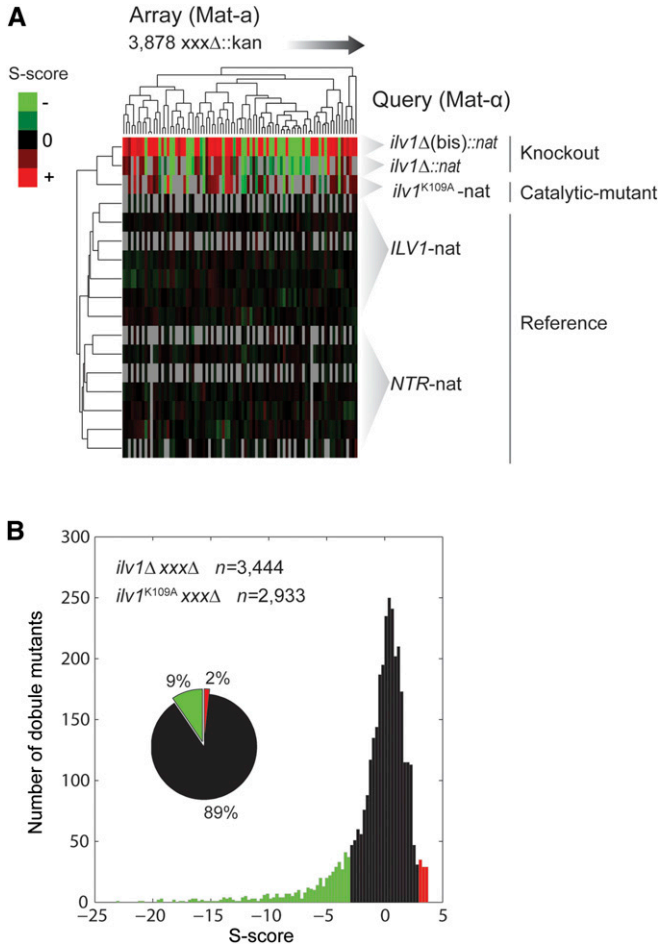

Figure 4 Epistasis-profile data analysis of *ILV1*. (A) Double-mutant and reference collections were generated by mating *MAT*α query strains of genome-integrated variants of *ILV1* with an array of *MAT***a** single-knockouts of most nonessential genes (see *Materials and Methods*). Heat-map shows hierarchical bidimensional clustering of array genes (*x*-axis) and query genes (*y*-axis) by their S-score profiles. Clustering was performed by average linkage with a Spearman's rank similarity metric using Gene Cluster 3.0; only a small subset of array genes is shown. (B) Histogram of S-scores from filtered data of the knockout and catalytic mutant strain collections (*ilv1*Δ *xxx*Δ and *ilv1*^{K109A} *xxx*Δ). Negative (green) and positive (red) genetic interactions in either collection are shown, as defined with a cutoff of |S-score| > 3.

tested). This result indicates that noncatalytic phenotypes are a feature of a limited set of genes encoding enzymes with possible moonlighting activities. Conversely, several genes showed consistent catalytic phenotypes across the conditions tested. Such was the case for knockouts of *ARO3*, *ARO4*, *ASN1*, *ASN2*, *HOM6*, and *THR4* (see Figure S4 for examples). Catalytic profiles in which the sole loss of catalysis explains all or most growth phenotypes indicate a single molecular function, that is, a monofunctional protein, at least under the limited set of conditions tested.

Our screen included strains in which the corresponding duplicate gene was deleted, which allowed us to test whether the presence of the paralog was masking the mutants' phenotypic effect. Indeed, duplicate genes *ALT1*, *ARO3*, *ARO4*, *ASN1*, and *ASN2* showed few growth phenotypes when analyzed in a single-gene knockout background. However, we observed more phenotypic diversity when the analysis was carried out in a double-knockout background (Figure 3C). For instance, the *aro3*Δ single knockout had no phenotype under most conditions tested, but the double *aro3*Δ*aro4*Δ strain grew slowly under many conditions, which allowed us to describe the catalytic nature of the Aro3-depletion phenotype. Likewise, more phenotypes were scored in the *alt1*Δ*alt2*Δ double knockout compared to the single *alt1*Δ. Intriguingly, the exposed phenotypes were mostly noncatalytic; this is consistent with a lack of catalytic activity in the Alt2 paralog (Peñalosa-Ruiz *et al.* 2012). These results suggest that a moonlighting noncatalytic function is present in Alt1 and shared with its paralog. Overall, our phenotypic screen allowed us to identify a set of phenotypes that do not depend on catalysis, underscoring additional relevant functions of yeast enzymes.

The noncatalytic genetic landscape of ILV1

To gain insight into the noncatalytic functions of one of the exposed moonlighting proteins, we focused on the genetic interactions of the *ILV1*-encoded threonine deaminase. This enzyme showed some of the strongest noncatalytic phenotypes in our screen. Measuring genetic interactions (epistasis), defined as the phenomenon in which the phenotype of a gene mutation is modified by the mutation of another gene, is a powerful way to reveal functional associations among genes (Segre *et al.* 2005; Boone *et al.* 2007; Costanzo *et al.* 2016). In particular, we generated a differential epistasis profile analysis (Bandyopadhyay *et al.* 2010; Braberg *et al.* 2013) of knockout and catalytic variants of *ILV1* to describe the dependency on catalysis of its genetic interactions.

We generated genome-integrated constructs of wild-type (*ilv1*Δ::*ILV1-NAT*), knockout (*ilv1*Δ::*NAT*), and catalytic mutant (*ilv1*Δ::*iv1*^{K109A}*-NAT*) strains. We mated each of these query strains to an array of 3878 nonessential gene knockouts to finally obtain collections of double-mutant haploids (Figure 4A). Based on the colony sizes of the double mutants compared to those of the corresponding single-knockout references, we obtained an S-score as a parameter of the magnitude and statistical confidence of each genetic interaction (Collins *et al.* 2006, 2010). Our epistasis profiles included an alternative reference strain with a different neutral marker insertion site and an additional *ilv1*Δ strain with a different gene deletion design (see *Materials and Methods*). Different query strain libraries clustered as expected in terms of their S-score profiles (Figure 4A), while all mutant strains were similar in terms of colony size variation within technical replicates (Figure S6). The distribution of S-scores of both mutant collections (*ilv1*Δ and *ilv1*^{K109A}) was centered at zero, with a short tail of positive (alleviating) and a long tail of negative (aggravating) genetic interactions (Figure 4B). Genetic interactions were defined using a fixed cutoff of |S-score| > 3 (Bandyopadhyay *et al.* 2010) in both double-mutant collections. Using this criterion, we found that in the combination of both mutant collections, 9% of double mutants resulted in negative interactions, while positive interactions were scored in 2% of cases (Figure 4B and

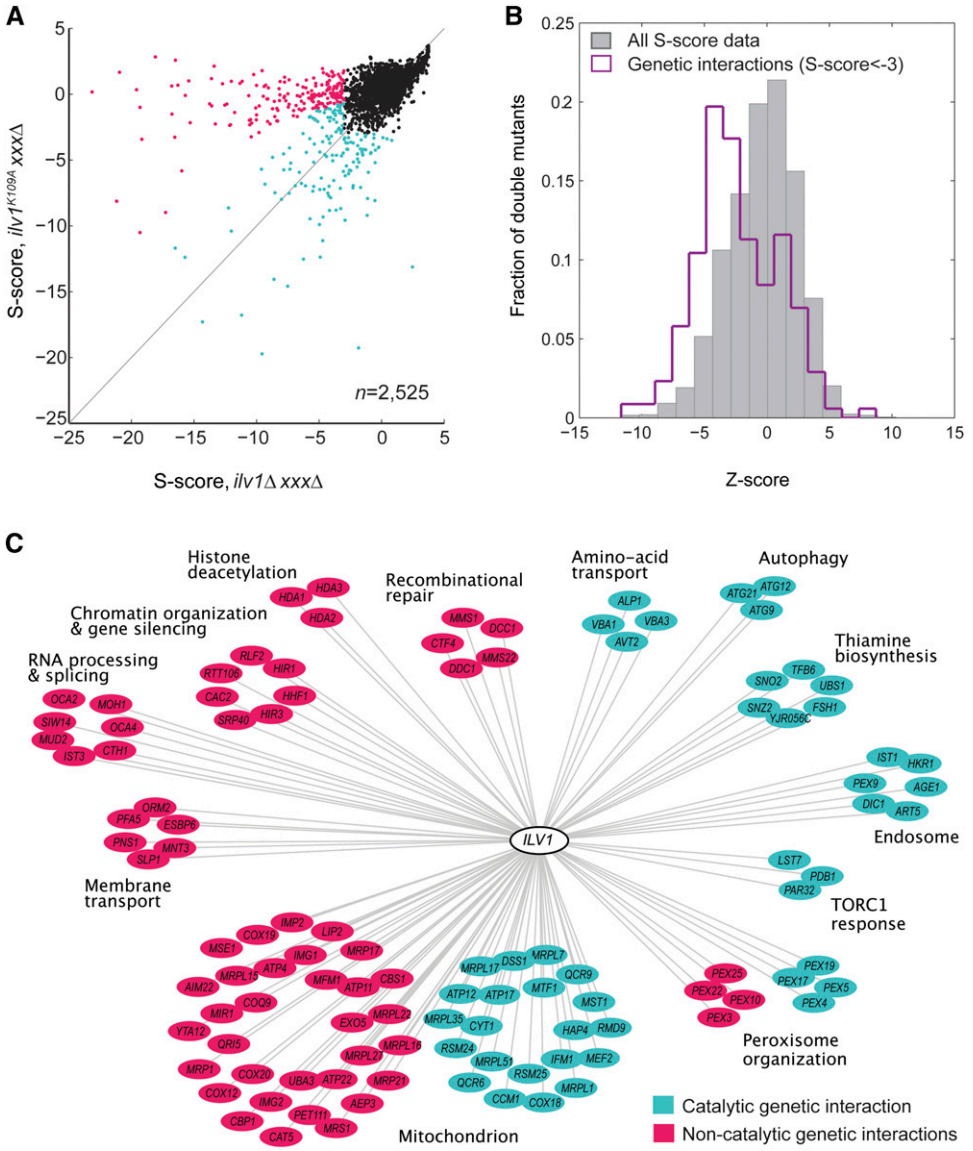

Figure 5 A set of genetic interactions of *ILV1* are not driven by loss of catalysis. (A) A differential epistasis profile analysis of knockout and catalytic mutants of *ILV1*. Scatter plots of S-scores for the *ilv1*Δ knockout (horizontal axis) and the *ilv1*^{K109A} catalytic mutant (vertical axis) collections. Negative genetic interactions were defined by S-score < -3 in either collection. Noncatalytic genetic interactions (magenta) were scored based on a stronger negative S-score of the knockout ($P < 0.005$). Negative genetic interactions with no significant difference (catalytic interactions) are shown in cyan. (B) Histogram of *Z*-scores of all compared gene pairs (gray bars) and gene pairs with significant negative genetic interactions (purple line). (C) Network representation of functional modules ($\kappa > 0.35$) of genes with noncatalytic (magenta) or catalytic (cyan) genetic interactions with *ILV1*.

File S2). These genetic interactions were enriched primarily in genes of metabolism, mitochondrial function, and chromatin organization (Table S5).

To describe the catalytic dependency of the genetic interaction landscape of *ILV1*, we compared the S-score profiles of the *ilv1*Δ and *ilv1*^{K109A} collections (Figure 5A). Strikingly, we observed a wide dispersion of S-scores above the diagonal, indicating that the strength of some negative genetic interactions in the *ilv1*Δ knockout was diminished in the *ilv1*^{K109A} catalytic mutant. This trend was not observed when contrasting the S-scores of the two different knockout strains [*ilv1*Δ and *ilv1*Δ(bis); Figure S7A]. These results suggested that an important number of genetic interactions of *ILV1* do not depend on loss of its catalytic activity.

To identify the specific cases of noncatalytic genetic interactions of *ILV1*, we performed a differential epistasis profile analysis by defining a *Z*-score of the difference in the corresponding S-scores (Figure S7B). We focused only on negative interactions, to avoid overscoring of marginal differences that could result from the narrow dynamic range of the positive genetic interaction spectrum. The *Z*-scores of genes with negative genetic interactions were skewed to negative values (Figure 5B). Indeed, we found 187 (54.2%) noncatalytic interactions out of 345 negative gene interactions ($P < 0.005$); the remaining 158 were defined as catalytic interactions.

Noncatalytic genetic interactions could arise from atypical features of the *ilv1*^{K109A} collection leading to a bias toward positive S-scores. Therefore, we inspected the colony sizes and their coefficients of variation in the double mutants (Figure S7C), which indicated that noncatalytic genetic interactions did not depend on unusually large colonies (leading to positive S-scores) or unusually high SD (resulting in S-scores close to zero). In sum, these observations reveal that around one half of the genetic interactions of *ILV1* do not depend solely on its catalytic activity, suggesting that, indeed, such noncatalytic interactions are driven by the phenotypes arising from the loss of moonlighting activities of *ILV1*.

To describe the cellular functions associated with both interaction categories, namely catalytic and noncatalytic genetic

interactions, we grouped genes from each category separately according to their shared GO-terms and mutant–phenotype annotations ($\kappa < 0.35$; Figure 5C). Both catalytic and noncatalytic hits were grouped in modules of genes with mitochondrial and peroxisome function, while catalytic hits resulted in clusters of genes involved in amino acid transport, autophagy, and TOR1-mediated response. Interestingly, many noncatalytic hits were clustered in different modules of genes with no direct connection to amino acid metabolism, RNA processing and splicing, chromatin organization, gene silencing, and the HDA1 complex. Such functional noncatalytic connections of *ILV1* to chromatin modification were also observed by GO term enrichment analysis (Table S6). The genetic interactions of the *ILV1* deletion with genes of chromatin regulation had been scored before in genome-wide epistasis screens (Costanzo *et al.* 2016). Remarkably, the genetic interaction profiles of *ILV1* with chromatin remodelers is similar to those of genes involved in the stress response (*RIM13*, *RIM20*, and *WHI2*), protein sorting (*SPR3*, *CHS5*, and *SEC63*), and chromatin remodeling (*ISW2* and *POB3*), but not to those of other metabolic genes (Bellay *et al.* 2011). Taken together, these observations indicate that the noncatalytic moonlighting activity of *ILV1* is associated with gene regulation, specifically to chromatin modification, in response to stress and other stimuli.

Discussion

Molecular biology has undergone a paradigm shift from the one gene–one function hypothesis while genetics and genomics have provided systems views of genes and proteins in their cellular context. Even though these advancements have led to the awareness of different types of gene multifunctionality, we are still on a quest to identify and reveal their underlying molecular and cellular mechanisms. Here, we focused on amino acid biosynthesis metabolism as a model system and dissected the gene deletion phenotypes of enzymes into those that can be explained by the loss of catalysis and those that cannot. We screened the phenotypic profiles of *S. cerevisiae* gene deletion, catalytic mutant, and reference strains, and found that as many as one-third of the genes tested showed frequent noncatalytic phenotypes. Such cases, in which loss of the catalytic function did not recapitulate loss of the corresponding enzyme, suggest proteins with a moonlighting behavior, and were prevalent in four enzymes: Alt1, Bat2, Ilv1, and Ilv2.

Our finding that most gene deletion phenotypes tested were driven by their catalytic function is in agreement with the view that genetic pleiotropy is usually caused by the perturbation of a single molecular function that affects many different cellular traits (He and Zhang 2006). Nonetheless, identifying noncatalytic functions could be challenging in conditions of strong dependence on the catalytic function. For example, the branched-chain amino acid transaminase Bat2 showed noncatalytic phenotypes in the single-gene knockout, which were rendered strongly catalytic in the double *bat1*Δ *bat2*Δ background. Moreover, mutations in *HOM6* and *THR4* are known to be highly pleiotropic because of the accumulation of toxic metabolic intermediates (Arévalo-Rodríguez *et al.* 2004; Kingsbury and McCusker 2010). In such cases, additional mutations in the metabolic pathway would provide a better means to interrogate the extent to which pleiotropy is explained solely by catalysis. Genes with consistent catalytic profiles in our screen should therefore be considered monofunctional until proven otherwise.

Four out of 11 amino acid biosynthesis enzymes tested showed a moonlighting behavior. Previous studies have suggested that the moonlighting hits in our screen could indeed have more than one molecular function. For instance, early studies had proposed that the *ILV1*-encoded enzyme from yeast is a multifunctional protein involved both in catalysis and in the regulation of the expression of genes of isoleucine and valine biosynthesis (Bollon and Magee 1971; Calhoun 1976). In addition, Bat1 and Bat2 control TORC1 signaling through a noncatalytic structural function (Kingsbury *et al.* 2015). Interestingly, the branched-chain aminotransferases have been retained throughout the evolution of metazoans, even though the anabolic pathways in which they participate have been lost; this is also the case for Ilv2, also identified as a moonlighting protein in our screen (Costa *et al.* 2015). We also note that the alanine transaminase Alt1 is a regulator of yeast chronological life span through metabolic flux control (Yu *et al.* 2013), but whether catalysis is enough for this biological role has not yet been directly addressed.

The quantitative nature of our genetic screen allowed us to identify some cases in which catalysis contributed partially to a "noncatalytic" phenotype. Moonlighting proteins are usually defined as molecules with two or more activities that are independent from one another (Huberts and van der Klei 2010; Zanzoni *et al.* 2015; Khan and Kihara 2016); however, our observations suggest that such activities may sometimes not be completely uncoupled. Partial functional contribution to phenotypes would be expected if two molecular activities in one protein cross talk to each other in the broader cellular context, for example in the case of enzymes that moonlight by acting as direct transcriptional regulators of genes in the same metabolic pathway (Meyer *et al.* 1991; Moore *et al.* 2003). Alternatively, single site-directed mutations affecting two molecular activities in moonlighting proteins could result in partial phenotypic contributions. The quantitative genetic description of moonlighting proteins will provide further understanding of how multiple activities originate, coexist, and evolve in a single polypeptide.

Databases of biological interaction networks contain valuable information that could help predict moonlighting functions (Khan *et al.* 2014; Chapple *et al.* 2015). Here, we show that genetic interaction screens of site-directed mutants provide a powerful means to uncover mechanisms of protein multifunctionality. The differential epistasis profile analysis of *ILV1* allowed us to shed light on the cellular role of its moonlighting function. We found noncatalytic interactions of *ILV1* with genes involved in chromatin organization and regulation, some of which have had been scored before in genome-wide epistasis screens (Costanzo *et al.* 2016). We

propose that the noncatalytic moonlighting activity of *ILV1* is associated with gene regulation, specifically to chromatin modification in response to stress and other stimuli. In addition, it is known that Ilv1 forms complexes with proteins involved in transcription, DNA maintenance, and chromatin structure (such as Rad51, Cpa2, Hsc82, and Rvb2), and interacts physically with proteins involved in protein folding and stress the response (Ssa1, Ssc1, Hsp6, Hsc82, and Hsp82) (Chatr-Aryamontri *et al.* 2017). It remains to be tested whether such physical interactions are required for the moonlighting behavior observed in Ilv1.

We note that other sources of gene multifunctionality—alternative splicing, alternative transcription sites, and post-transcriptional modification—and not actual protein moonlighting may underlie the noncatalytic phenotypes scored in our screen. In addition, we have verified that catalysis of site-directed mutants is compromised only to the extent of inhibiting growth in minimal media on the timescale of the experiment. Nonetheless, residual activity might result in the complementation of the knockout phenotypes in different biological contexts. Under this scenario, the observed multifunctionality would be explained by a mechanism different from protein moonlighting, where the fitness and epistasis landscapes would be qualitatively modulated by a single, quantitative molecular function.

In conclusion, our study shows that the gene loss phenotypes of metabolic enzymes frequently do not depend on an annotated catalytic activity. We have learned that the chance of uncover proteins with such moonlighting behavior is related to the magnitude, frequency, and regularity of the phenotype under different cellular contexts and our ability to detect and measure it. These characteristics, in turn, depend on genetic redundancy, the degree of molecular and phenotypic interdependence between functions in a single polypeptide, and the dominance of the phenotypes associated with multifunctionality. Even though we focused on enzymes, our strategy can be readily used to identify other types of potentially multifunctional proteins. Most likely, numerous moonlighting proteins within and beyond metabolism are yet to be discovered and characterized, providing a deeper understanding of cell biology, from metabolism and functional annotation to single gene and complex traits.

Acknowledgments

We thank C. Abreu-Goodger and F. Barona-Gómez for help with statistical analyses and catalytic mutant design, respectively, and to C. Abreu-Goodger and E. Mancera for critical reading of the manuscript. Strain BUN20 and plasmid p5586 were kindly shared by Charles Boone's laboratory. This work was funded by the Consejo Nacional de Ciencia y Tecnología de México (CONACYT, grant CB2015/164889 to A.D.) and the University of California Institute for Mexico and the US (UC MEXUS-COANCYT grant CN15-48 to A.D.). A.E.-C. had a doctoral fellowship from CONACYT (grant 230319). The funders had no role in study design, data collection and analysis, the decision to publish, or preparation of the manuscript.

Literature Cited

Amberg, D. C, D. J. Burke, and J. N. Strathern, 2005 Methods in Yeast Genetics: A Cold Spring Harbor Laboratory Course Manual. Cold Spring Harbor (New York): Cold Spring Harbor Laboratory Press.

Arévalo-Rodríguez, M., X. Pan, J. D. Boeke, and J. Heitman, 2004 FKBP12 controls aspartate pathway flux in Saccharomyces cerevisiae to prevent toxic intermediate accumulation. Eukaryot. Cell 3: 1287–1296.

Ashburner, M., C. A. Ball, J. A. Blake, D. Botstein, H. Butler *et al.*, 2000 Gene ontology: tool for the unification of biology. Nat. Genet. 25: 25.

Baliga, N. S., J. L. Björkegren, J. D. Boeke, M. Boutros, N. P. Crawford *et al.*, 2017 The state of systems genetics in 2017. Cell Syst. 4: 7–15.

Bandyopadhyay, S., M. Mehta, D. Kuo, M. K. Sung, R. Chuang *et al.*, 2010 Rewiring of genetic networks in response to DNA damage. Science 330: 1385–1389.

Bellay, J., G. Atluri, T. L. Sing, K. Toufighi, M. Costanzo *et al.*, 2011 Putting genetic interactions in context through a global modular decomposition. Genome Res. 21: 1375–1387.

Benjamini, Y., and Y. Hochberg, 1995 Controlling the false discovery rate: a practical and powerful approach to multiple testing. J. R. Stat. Soc. B 57: 289–300.

Bienert, S., A. Waterhouse, T. A. de Beer, G. Tauriello, G. Studer *et al.*, 2017 The SWISS-MODEL Repository—new features and functionality. Nucleic Acids Res. 45: D313–D319.

Bollon, A. P., and P. T. Magee, 1971 Involvement of threonine deaminase in multivalent repression of the isoleucine-valine pathway in Saccharomyces cerevisiae. Proc. Natl. Acad. Sci. USA 68: 2169–2172.

Boone, C., H. Bussey, and B. J. Andrews, 2007 Exploring genetic interactions and networks with yeast. Nat. Rev. Genet. 8: 437–449.

Boukouris, A. E., S. D. Zervopoulos, and E. D. Michelakis, 2016 Metabolic enzymes moonlighting in the nucleus: metabolic regulation of gene transcription. Trends Biochem. Sci. 41: 712–730.

Braberg, H., H. Jin, E. A. Moehle, Y. A. Chan, S. Wang *et al.*, 2013 From structure to systems: high-resolution, quantitative genetic analysis of RNA polymerase II. Cell 154: 775–788.

Calhoun, D. H., 1976 Threonine deaminase from Escherichia coli: feedback-hypersensitive enzyme from a genetic regulatory mutant. J. Bacteriol. 126: 56–63.

Carter, G. W., 2013 Inferring gene function and network organization in Drosophila signaling by combined analysis of pleiotropy and epistasis. G3 (Bethesda) 3: 807–814.

Chapple, C. E., B. Robisson, L. Spinelli, C. Guien, E. Becker *et al.*, 2015 Extreme multifunctional proteins identified from a human protein interaction network. Nat. Commun. 6: 7412.

Chatr-Aryamontri, A., R. Oughtred, L. Boucher, J. Rust, C. Chang *et al.*, 2017 The BioGRID interaction database: 2017 update. Nucleic Acids Res. 45: D369–D379.

Chen, X. J., X. Wang, B. A. Kaufman, and R. A. Butow, 2005 Aconitase couples metabolic regulation to mitochondrial DNA maintenance. Science 307: 714–717.

Collins, S. R., M. Schuldiner, N. J. Krogan, and J. S. Weissman, 2006 A strategy for extracting and analyzing large-scale quantitative epistatic interaction data. Genome Biol. 7: R63.

Collins, S. R., A. Roguev, and N. J. Krogan, 2010 Quantitative genetic interaction mapping using the E-MAP approach. Methods Enzymol. 470: 205–231.

Commichau, F. M., and J. Stülke, 2008 Trigger enzymes: bifunctional proteins active in metabolism and in controlling gene expression. Mol. Microbiol. 67: 692–702.

Copley, S. D., 2003 Enzymes with extra talents: moonlighting functions and catalytic promiscuity. Curr. Opin. Chem. Biol. 7: 265–272.

Copley, S. D., 2012 Moonlighting is mainstream: paradigm adjustment required. BioEssays 34: 578–588.
Costa, I., J. Thompson, J. Ortega, and F. Prosdocimi, 2015 Metazoan remaining genes for essential amino acid biosynthesis: sequence conservation and evolutionary analyses. Nutrients 7: 1–16.
Costanzo, M., B. Vandersluis, E. N. Koch, A. Baryshnikova, C. Pons *et al.*, 2016 A global genetic interaction network maps a wiring diagram of cellular function. Science 353: aaf1420.
DeLaBarre, B., P. R. Thompson, G. D. Wright, and A. M. Berghuis, 2000 Crystal structures of homoserine dehydrogenase suggest a novel catalytic mechanism for oxidoreductases. Nat. Struct. Biol. 7: 238–244.
DeLuna, A., K. Vetsigian, N. Shoresh, M. Hegreness, M. Colón-González *et al.*, 2008 Exposing the fitness contribution of duplicated genes. Nat. Genet. 40: 676.
Deutschbauer, A., M. N. Price, K. M. Wetmore, D. R. Tarjan, Z. Xu *et al.*, 2014 Towards an informative mutant phenotype for every bacterial gene. J. Bacteriol. 196: 3643–3655.
Dudley, A. M., D. M. Janse, A. Tanay, R. Shamir, and G. M. Church, 2005 A global view of pleiotropy and phenotypically derived gene function in yeast. Mol. Syst. Biol. 1: 2005.0001.
Eden, E., R. Navon, I. Steinfeld, D. Lipson, and Z. Yakhini, 2009 GOrilla: a tool for discovery and visualization of enriched GO terms in ranked gene lists. BMC Bioinformatics 10: 48.
Entelis, N., I. Brandina, P. Kamenski, I. A. Krasheninnikov, R. P. Martin *et al.*, 2006 A glycolytic enzyme, enolase, is recruited as a cofactor of tRNA targeting toward mitochondria in Saccharomyces cerevisiae. Genes Dev. 20: 1609–1620.
Espinosa-Cantú, A., D. Ascencio, F. Barona-Gómez, and A. DeLuna, 2015 Gene duplication and the evolution of moonlighting proteins. Front. Genet. 6: 227.
Fisher, K. E., and E. Eisenstein, 1993 An efficient approach to identify ilvA mutations reveals an amino-terminal catalytic domain in biosynthetic threonine deaminase from Escherichia coli. J. Bacteriol. 175: 6605–6613.
Furnham, N., G. L. Holliday, T. A. P. De Beer, J. O. B. Jacobsen, W. R. Pearson *et al.*, 2014 The Catalytic Site Atlas 2.0: cataloging catalytic sites and residues identified in enzymes. Nucleic Acids Res. 42: D485–D489.
Gancedo, C., and C.-L. Flores, 2008 Moonlighting proteins in yeasts. Microbiol. Mol. Biol. Rev. 72: 197–210.
Garay, E., S. E. Campos, J. González De La Cruz, A. P. Gaspar, A. Jinich *et al.*, 2014 High-resolution profiling of stationary-phase survival reveals yeast longevity factors and their genetic interactions. PLoS Genet. 10: e1004168.
Guillaume, F., and S. P. Otto, 2012 Gene functional trade-offs and the evolution of pleiotropy. Genetics 192: 1389–1409.
Hall, D. A., H. Zhu, X. Zhu, T. Royce, M. Gerstein *et al.*, 2004 Regulation of gene expression by a metabolic enzyme. Science 306: 482–484.
Hampsey, M., 1997 A review of phenotypes in Saccharomyces cerevisiae. Yeast 13: 1099–1133.
He, X., and J. Zhang, 2006 Toward a molecular understanding of pleiotropy. Genetics 173: 1885–1891.
Henderson, B., and A. Martin, 2013 Bacterial moonlighting proteins and bacterial virulence, pp. 155–213 in *Between Pathogenicity and Commensalism*, edited by U. Dobrindt, J. H. Hacker, and C. Svanborg. Springer, Berlin.
Hernández, S., G. Ferragut, I. Amela, J. Perez-Pons, J. Piñol *et al.*, 2014 MultitaskProtDB: a database of multitasking proteins. Nucleic Acids Res. 42: D517–D520.
Hernández, S., L. Franco, A. Calvo, G. Ferragut, A. Hermoso *et al.*, 2015 Bioinformatics and moonlighting proteins. Front. Bioeng. Biotechnol. 3: 90.
Hill, N. S., P. J. Buske, Y. Shi, and P. A. Levin, 2013 A moonlighting enzyme links Escherichia coli cell size with central metabolism. PLoS Genet. 9: e1003663.
Hill, W. G., and X.-S. Zhang, 2012 Assessing pleiotropy and its evolutionary consequences: pleiotropy is not necessarily limited, nor need it hinder the evolution of complexity. Nat. Rev. Genet. 13: 296.
Hillenmeyer, M. E., E. Fung, J. Wildenhain, S. E. Pierce, S. Hoon *et al.*, 2008 The chemical genomic portrait of yeast: uncovering a phenotype for all genes. Science 320: 362–365.
Ho, C. H., L. Magtanong, S. L. Barker, D. Gresham, S. Nishimura *et al.*, 2009 A molecular barcoded yeast ORF library enables mode-of-action analysis of bioactive compounds. Nat. Biotechnol. 27: 369–377.
Hodgkin, J., 1998 Seven types of pleiotropy. Int. J. Dev. Biol. 42: 501–505.
Holliday, G. L., C. Andreini, J. D. Fischer, S. A. Rahman, D. E. Almonacid *et al.*, 2012 MACiE: exploring the diversity of biochemical reactions. Nucleic Acids Res. 40: D783–D789.
Huberts, D. H., and I. J. Van Der Klei, 2010 Moonlighting proteins: an intriguing mode of multitasking. Biochim. Biophys. Acta 1803: 520–525.
Hughes, T. R., C. J. Roberts, H. Dai, A. R. Jones, M. R. Meyer *et al.*, 2000 Widespread aneuploidy revealed by DNA microarray expression profiling. Nat. Genet. 25: 333–337.
Ittisoponpisan, S., E. Alhuzimi, M. J. E. Sternberg, and A. David, 2017 Landscape of pleiotropic proteins causing human disease: structural and system biology insights. Hum. Mutat. 38: 289–296.
Jeffery, C. J., 1999 Moonlighting proteins. Trends Biochem. Sci. 24: 8–11.
Jeffery, C. J., 2011 Proteins with neomorphic moonlighting functions in disease. IUBMB Life 63: 489–494.
Jeffery, C. J., 2015 Why study moonlighting proteins? Front. Genet. 6: 211.
Jensen, R. A., 1976 Enzyme recruitment in evolution of new function. Annu. Rev. Microbiol. 30: 409–425.
Khan, I., Y. Chen, T. Dong, X. Hong, R. Takeuchi *et al.*, 2014 Genome-scale identification and characterization of moonlighting proteins. Biol. Direct 9: 30.
Khan, I. K., and D. Kihara, 2016 Genome-scale prediction of moonlighting proteins using diverse protein association information. Bioinformatics 32: 2281–2288.
Khersonsky, O., and D. S. Tawfik, 2010 Enzyme promiscuity: a mechanistic and evolutionary perspective. Annu. Rev. Biochem. 79: 471–505.
Khersonsky, O., C. Roodveldt, and D. S. Tawfik, 2006 Enzyme promiscuity: evolutionary and mechanistic aspects. Curr. Opin. Chem. Biol. 10: 498–508.
Kingsbury, J. M., and J. H. McCusker, 2010 Homoserine toxicity in Saccharomyces cerevisiae and Candida albicans homoserine kinase (thr1Delta) mutants. Eukaryot. Cell 9: 717–728.
Kingsbury, J. M., N. D. Sen, and M. E. Cardenas, 2015 Branched-chain aminotransferases control TORC1 signaling in Saccharomyces cerevisiae. PLoS Genet. 11: e1005714.
Kirschner, K., and H. Bisswanger, 1976 Multifunctional proteins. Annu. Rev. Biochem. 45: 143–166.
Li, M. Z., and S. J. Elledge, 2005 MAGIC, an in vivo genetic method for the rapid construction of recombinant DNA molecules. Nat. Genet. 37: 311–319.
Mani, M., C. Chen, V. Amblee, H. Liu, T. Mathur *et al.*, 2015 MoonProt: a database for proteins that are known to moonlight. Nucleic Acids Res. 43: D277–D282.
Meyer, J., A. Walker-Jonah, and C. P. Hollenberg, 1991 Galactokinase encoded by GAL1 is a bifunctional protein required for induction of the GAL genes in Kluyveromyces lactis and is able to suppress the gal3 phenotype in Saccharomyces cerevisiae. Mol. Cell. Biol. 11: 5454–5461.
Moore, B., L. Zhou, F. Rolland, Q. Hall, W.-H. Cheng *et al.*, 2003 Role of the Arabidopsis glucose sensor HXK1 in nutrient, light, and hormonal signaling. Science 300: 332–336.

Norman, K. L., and A. Kumar, 2016 Mutant power: using mutant allele collections for yeast functional genomics. Brief. Funct. Genomics 15: 75–84.
Ohya, Y., J. Sese, M. Yukawa, F. Sano, Y. Nakatani *et al.*, 2005 High-dimensional and large-scale phenotyping of yeast mutants. Proc. Natl. Acad. Sci. USA 102: 19015–19020.
Paaby, A. B., and M. V. Rockman, 2013 The many faces of pleiotropy. Trends Genet. 29: 66–73.
Peñalosa-Ruiz, G., C. Aranda, L. Ongay-Larios, M. Colon, H. Quezada *et al.*, 2012 Paralogous ALT1 and ALT2 retention and diversification have generated catalytically active and inactive aminotransferases in Saccharomyces cerevisiae. PLoS One 7: e45702.
Peracchi, A., 2001 Enzyme catalysis: removing chemically 'essential' residues by site-directed mutagenesis. Trends Biochem. Sci. 26: 497–503.
Piatigorsky, J., 2007 *Gene Sharing and Evolution*. Harvard University Press, Cambridge, MA.
Pollard, T. D., 2003 Functional genomics of cell morphology using RNA interference: pick your style, broad or deep. J. Biol. 2: 25.
Pritykin, Y., D. Ghersi, and M. Singh, 2015 Genome-wide detection and analysis of multifunctional genes. PLOS Comput. Biol. 11: e1004467.
Promislow, D., 2004 Protein networks, pleiotropy and the evolution of senescence. Proc. R. Soc. Lond. B Biol. Sci. 271: 1225–1234.
Scherrer, T., N. Mittal, S. C. Janga, and A. P. Gerber, 2010 A screen for RNA-binding proteins in yeast indicates dual functions for many enzymes. PLoS One 5: e15499.
Schiestl, R. H., and R. D. Gietz, 1989 High efficiency transformation of intact yeast cells using single stranded nucleic acids as a carrier. Curr. Genet. 16: 339–346.
Schnappauf, G., N. Sträter, W. N. Lipscomb, and G. H. Braus, 1997 A glutamate residue in the catalytic center of the yeast chorismate mutase restricts enzyme activity to acidic conditions. Proc. Natl. Acad. Sci. USA 94: 8491–8496.
Schuldiner, M., S. R. Collins, N. J. Thompson, V. Denic, A. Bhamidipati *et al.*, 2005 Exploration of the function and organization of the yeast early secretory pathway through an epistatic miniarray profile. Cell 123: 507–519.
Segre, D., A. Deluna, G. M. Church, and R. Kishony, 2005 Modular epistasis in yeast metabolism. Nat. Genet. 37: 77–83.
Shalem, O., N. E. Sanjana, and F. Zhang, 2015 High-throughput functional genomics using CRISPR-Cas9. Nat. Rev. Genet. 16: 299–311.
Shi, Y., and Y. Shi, 2004 Metabolic enzymes and coenzymes in transcription – a direct link between metabolism and transcription? Trends Genet. 20: 445–452.
Smith, S. D., 2016 Pleiotropy and the evolution of floral integration. New Phytol. 209: 80–85.
Song, P., H. Wei, Z. Cao, P. Wang, and G. Zhu, 2014 Single arginine mutation in two yeast isocitrate dehydrogenases: biochemical characterization and functional implication. PLoS One 9: e115025.
Sriram, G., J. A. Martinez, E. R. B. McCabe, J. C. Liao, and K. M. Dipple, 2005 Single-gene disorders: what role could moonlighting enzymes play? Am. J. Hum. Genet. 76: 911–924.
Stearns, F. W., 2010 One hundred years of pleiotropy: a retrospective. Genetics 186: 767–773.
Supek, F., M. Bošnjak, N. Škunca, and T. Šmuc, 2011 REVIGO summarizes and visualizes long lists of gene ontology terms. PLoS One 6: e21800.
Szappanos, B., K. Kovács, B. Szamecz, F. Honti, M. Costanzo *et al.*, 2011 An integrated approach to characterize genetic interaction networks in yeast metabolism. Nat. Genet. 43: 656–662.
Tokuriki, N., and D. S. Tawfik, 2009 Stability effects of mutations and protein evolvability. Curr. Opin. Struct. Biol. 19: 596–604.
Torres-Machorro, A. L., J. P. Aris, and L. Pillus, 2015 A moonlighting metabolic protein influences repair at DNA double-stranded breaks. Nucleic Acids Res. 43: 1646–1658.
Wagner, G. P., and J. Zhang, 2011 The pleiotropic structure of the genotype–phenotype map: the evolvability of complex organisms. Nat. Rev. Genet. 12: 204–213.
Warringer, J., and A. Blomberg, 2003 Automated screening in environmental arrays allows analysis of quantitative phenotypic profiles in Saccharomyces cerevisiae. Yeast 20: 53–67.
Yoshida, N., K. Oeda, E. Watanabe, T. Mikami, Y. Fukita *et al.*, 2001 Protein function. Chaperonin turned insect toxin. Nature 411: 44.
Yu, S. L., Y. J. An, H. J. Yang, M. S. Kang, H. Y. Kim *et al.*, 2013 Alanine-metabolizing enzyme Alt1 is critical in determining yeast life span, as revealed by combined metabolomic and genetic studies. J. Proteome Res. 12: 1619–1627.
Zanzoni, A., C. E. Chapple, and C. Brun, 2015 Relationships between predicted moonlighting proteins, human diseases, and comorbidities from a network perspective. Front. Physiol. 6: 171.
Zelenaya-Troitskaya, O., P. S. Perlman, and R. A. Butow, 1995 An enzyme in yeast mitochondria that catalyzes a step in branched-chain amino acid biosynthesis also functions in mitochondrial DNA stability. EMBO J. 14: 3268–3276.
Zou, L., S. Sriswasdi, B. Ross, P. V. Missiuro, J. Liu *et al.*, 2008 Systematic analysis of pleiotropy in C. elegans early embryogenesis. PLOS Comput. Biol. 4: e1000003.

Communicating editor: L. Steinmetz